Research Article Vol. 8, No. 4 / April 2020 / Photonics Research 511

PHOTONICS Research

Passively Q-switched and femtosecond mode-locked erbium-doped fiber laser based on a 2D palladium disulfide (PdS_2) saturable absorber

Ping Kwong Cheng,† Chun Yin Tang,† Xin Yu Wang, Long-Hui Zeng, and Yuen Hong Tsang*

Department of Applied Physics and Materials Research Center, The Hong Kong Polytechnic University, Hung Hom, Kowloon, Hong Kong, China
**Corresponding author: Yuen. Tsang@polyu.edu.hk*

Received 11 October 2019; revised 26 December 2019; accepted 5 January 2020; posted 6 January 2020 (Doc. ID 380146); published 24 March 2020

Stable Q-switched and mode-locked erbium-doped fiber lasers (EDFLs) are first demonstrated by using the novel layered palladium disulfide (PdS_2), a new member of group 10 transition metal dichalcogenides (TMDs)-based saturable absorbers (SAs). Self-started Q-switched operation at 1567 nm was achieved with a threshold pump power of 50.6 mW. The modulation ranges of pulse duration and repetition rate were characterized as 12.6–4.5 μs and 17.2–26.0 kHz, respectively. Meanwhile, a mode-locked EDFL was also obtained with a pump power threshold of 106.4 mW. The achieved pulse duration is 803 fs, corresponding to a center wavelength of 1565.8 nm and 4.48 nm 3 dB bandwidth. To the best of our knowledge, the achieved pulse duration of the mode-locked EDFL in this work is the narrowest compared with all other group 10 TMD SA-based lasers.

https://doi.org/10.1364/PRJ.380146

1. INTRODUCTION

Pulsed lasers are extensively being applied in diverse modern technology fields, ranging from material processing [1,2], medical treatment [3,4], sensing, metrology [5], to scientific research [6–8]. Depending on the application, either the Q-switching or mode-locking technique is utilized to produce laser pulses with nano- to femtosecond duration. An acousto-optic modulator (AOM) [9] or an electro-optic modulator (EOM) [10] is used to generate laser pulses actively. However, these active modulators are bulky and costly. Comparatively, passive Q switching and mode locking based on saturable absorbers (SAs) would be a cost-effective technique for laser pulse generation.

An SA is a nonlinear optical (NLO) device whose transmittance can be modulated passively according to the incident light intensity. Semiconductor saturable absorber mirrors (SESAMs, e.g., InGaAs [11]) and doped crystal (e.g., Cr^{4+}:YAG [12]) were typically utilized for inducing passively mode-locked and Q-switched pulses, respectively. Nevertheless, their disadvantages of limited bandgap energy and complicated and expensive synthesis processes still limit the development of the pulsed laser [13]. Therefore, the exploration of substitutional SA materials with new features is a sustained quest in the NLO field. Graphene is one of the most prominent demonstrations of a broadband SA [14,15]. It also motivated the study of other graphene-like two-dimensional (2D) material SAs, for instance, graphene oxide [16,17], black phosphorus (BP) [18,19], as well as transition metal dichalcogenides (TMDs) [20]. TMDs are 2D materials that consist of MX_2 molecular structure, where M is the group 4–10 transition metal element (Nb, Mo, W) and X is the chalcogenide element (S, Se, Te). In recent years, TMDs have attracted huge interest due to their unique atomic structure, distinctive electrical and photonic properties, strong mechanical strength [21], high charge carrier mobility [22], and tunable electronic and photonic properties [23,24]. TMDs have been widely applied in various optoelectronic applications, ranging from photocatalysts [25] to field-effect transistors (FETs) [26] to photodetectors [27–30], and especially SAs (e.g., WS_2 [31,32] and MoS_2 [33]).

Recently, the newly developed platinum (Pt)- and palladium (Pd)-based group 10 layered materials have drawn enormous attention due to the merits of high mobility, remarkable NLO properties, and high air stability within an ambient environment [34]. The literature has demonstrated the ultrastable operations of $PtSe_2$- [26,27] and $PdSe_2$- [30,35,36] based optoelectronic devices in ambient conditions, which suggested the group 10 TMDs are a promising candidate for laser photonic applications. For the SA application, the works of Pt-based TMDs–SAs have been well demonstrated, including of PtS_2 [37,38], $PtSe_2$ [13,34,39,40], and $PtTe_2$ [41]. However, there is no report of ultrafast laser performance based on the Pd TMDs; therefore, it is worthwhile to further explore and investigate the nonlinear saturable absorption properties of these layered Pd TMDs. Palladium disulfide (PdS_2) is one of the most competitive candidates, with an interesting crystal structure and material properties. As shown in Fig. 1, PdS_2 has a pentagonal crystal structure

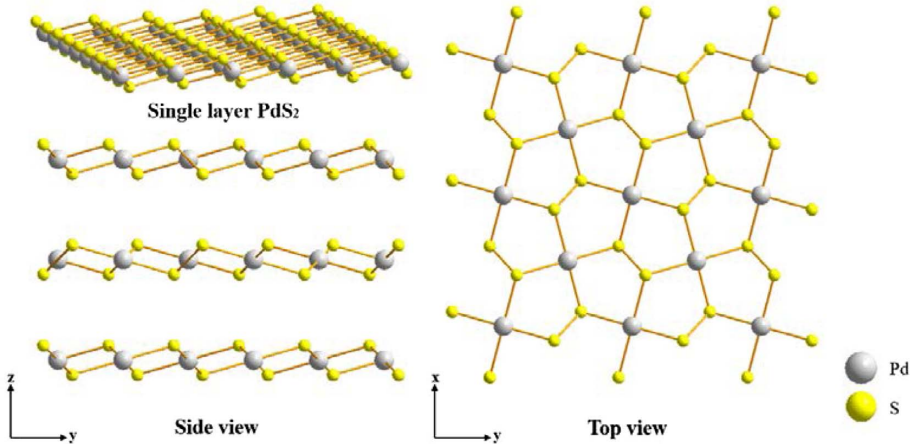

Fig. 1. Crystal structure of a layered PdS_2.

different from the hexagonal crystal structure of other TMD materials, such as MoS_2, WS_2, and PtS_2. Wang *et al.* reported the monolayer (ML) PdS_2 has a 1.6 eV indirect bandgap [42]. Bilayer (BL) to bulky PdS_2 exhibits the semimetallic property [43]. This unique electronic structure granted the PdS_2 multifunctional applicability. For instance, BL/ML/BL-PdS_2 structure has been proposed as a channel in the logical junction [43]. Meanwhile ML-PdS_2 is predicted to possess a strong photocatalytic ability for hydrogen and oxygen evolution reactions [44]. In this work, passively *Q*-switched and mode-locked EDFLs based on PdS_2-SA are successfully demonstrated. To the best of our knowledge, this is the first time for utilizing Pd-based TMDs as SAs for both *Q*-switching and mode-locking operations.

2. PdS_2 EXFOLIATION AND MATERIAL CHARACTERIZATION

PdS_2 powder (Six Carbon Inc.) was first mingled with isopropyl alcohol (IPA) solvent under a 1 mg/mL ratio. Then the mixture was sonicated at 40 kHz ultrasonic frequency and 400 W power for around 20 h. Afterward, the PdS_2-IPA supernatant was prepared by using the centrifugal method at 3000 r/min speed for 5 min, which could remove impurities and the bulk materials.

After the successful exfoliation, the PdS_2 samples were first characterized by utilizing field emission electron microscopy (FETEM, JEOL Model JEM-2100F). Figure 2(a) shows the transmission electron microscopy (TEM) observation of a

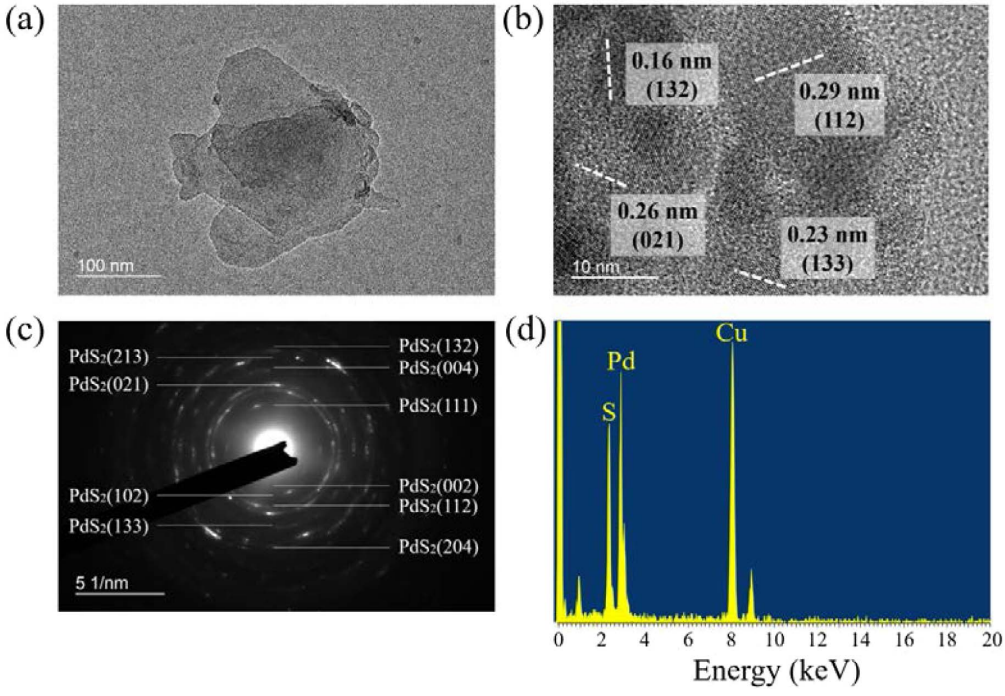

Fig. 2. (a) FETEM image and (b) corresponding high-resolution transmission electron microscopy (HRTEM) image of a randomly selected PdS_2 flake; (c) SAED pattern and (d) EDS profile of the PdS_2 sample.

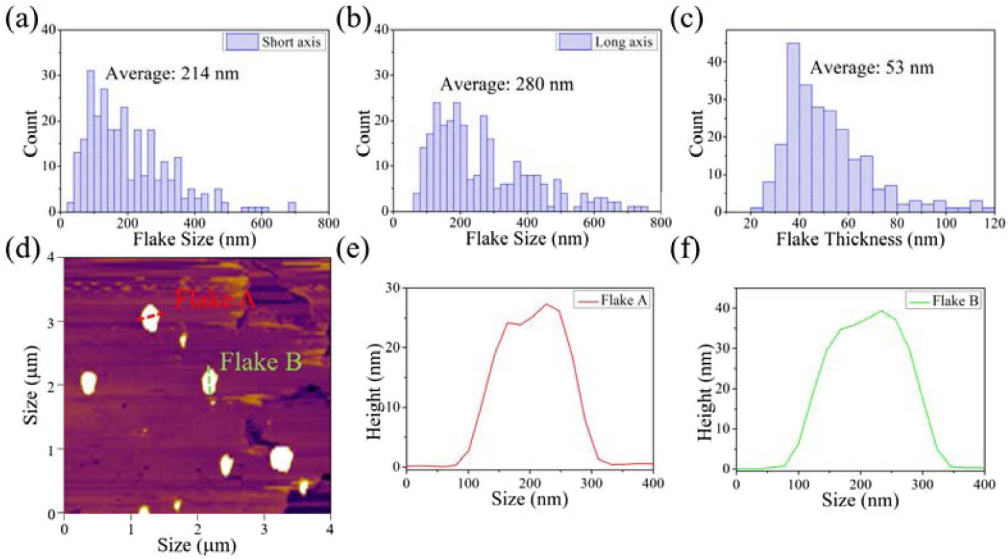

Fig. 3. Statistical distribution of lateral size along (a) short axis, (b) long axis, and (c) layer thickness (analyzed from 250 PdS_2 flake samples); (d) AFM image of measured PdS_2 flakes with respect to the height profile of (e) Flake A and (f) Flake B.

randomly selected PdS_2 flake whose lateral dimensions are about 250 nm (short axis) and 260 nm (long axis), respectively. In addition, from the high-resolution TEM observation [Fig. 2(b)], individual crystal lattice planes of PdS_2 flakes were quantified at (112), (021), (133), and (132) with the corresponding d-spacing of 0.29, 0.26, 0.23, and 0.16 nm, respectively [45]. Meanwhile, the crystallinity of the fabricated PdS_2 samples was also characterized by the selected area electron diffraction (SAED) pattern. Figure 2(c) has revealed several polymorphic rings that represent the PdS_2 crystal lattice planes (112), (021), (204), and (132); this suggested that the obtained sample is polycrystalline. The measured crystal lattice planes are in good agreement with the database of the Materials Project [37]. The energy-dispersive X-ray spectroscopy (EDS) profile of PdS_2 samples was measured and is shown in Fig. 2(d). There are no observable impurities (the signal of Cu is detected due to the copper mesh used in the FETEM measurement).

Atomic force microscopy (AFM, Bruker Nanoscope 8) was utilized to measure the topological characteristics of the PdS_2 flakes. The topological data among 250 flakes were analyzed; the average values of the lateral size along the short axis, long axis, and layer thickness are 214, 280, and 53 nm, respectively [Figs. 3(a)–3(c)]. As shown in Fig. 3(d), two flakes (Flake A and Flake B) were randomly selected from a topology graph to exhibit their height profiles [Figs. 3(e) and 3(f)]. The lateral sizes along the short axis of Flake A and the long axis of Flake B are about 200 and 250 nm, respectively, which agrees well with the TEM observation.

3. PULSED FIBER LASER SETUP

The setup of PdS_2-based passively *Q*-switched and mode-locked EDFL is presented in Fig. 4. The ring cavity is composed of a 976/1550 wavelength division multiplexer (WDM), polarization-independent isolator (PI-ISO), polarization controller (PC), 1:9 output coupler, erbium-doped single-mode fiber (EDF), and single-mode fiber (SMF). The total cavity length is about 12.36 m, which consists of a 0.7 m long EDF [LIEKKI Er 110-4/125, group velocity dispersion (GVD), 12 ps^2/km] and an 11.66 m SMF (SMF-28; GVD, −19 ps^2/km). In the experiment, two types of PdS_2-based SAs were tested; the results are discussed in the following section.

4. EXPERIMENTAL RESULTS AND DISCUSSION

In the experiment, the as-prepared PdS_2 samples were first incorporated into a polyvinyl alcohol (PVA) polymer to form a matrix composite. As shown in Fig. 4, the PdS_2-PVA composite thin film was inserted between the end surface of two fiber connectors to act as a transmission-type SA. *Q*-switched pulses with a center wavelength of 1567 nm were detected as the optical pump power scaled beyond a threshold value of 50.6 mW. For the pump power over 81.7 mW, the *Q*-switched pulses vanished and switched to continuous wave (CW) operation, which is due to the oversaturation of the SA [18,46]. The measured average output power ranged from 0.138 to 0.393 mW, as shown in Fig. 5(a). Moreover, the modulation ranges of repetition rate and the full width at half-maximum (FWHM) of pulse duration are 17.2 to 26.0 kHz and 12.6 to 4.5 μs, respectively [Figs. 5(b)–5(d)]. Meanwhile, the achieved maximum single-pulse energy is around 15.1 nJ. The radio-frequency (RF) spectrum of the *Q*-switched operation was measured with a resolution bandwidth of 40 Hz and is shown in Fig. 5(e). The signal-to-noise ratio (SNR) is up to 50 dB, which suggests a highly stable *Q*-switched performance. As shown in Table 1, the achieved minimum *Q*-switched pulse duration of 4.5 μs in this work is comparable to other group 10 TMD SA-based results (PtS_2, 4.2 μs [38]; $PtSe_2$, 0.9 μs [39]; $PtTe_2$, 5.2 μs [41]), and supports the notion that PdS_2 is a competitive candidate for use as a nonlinear SA device.

To further explore the nonlinear saturable absorption properties of the fabricated PdS_2 samples, an alternative SA synthesis

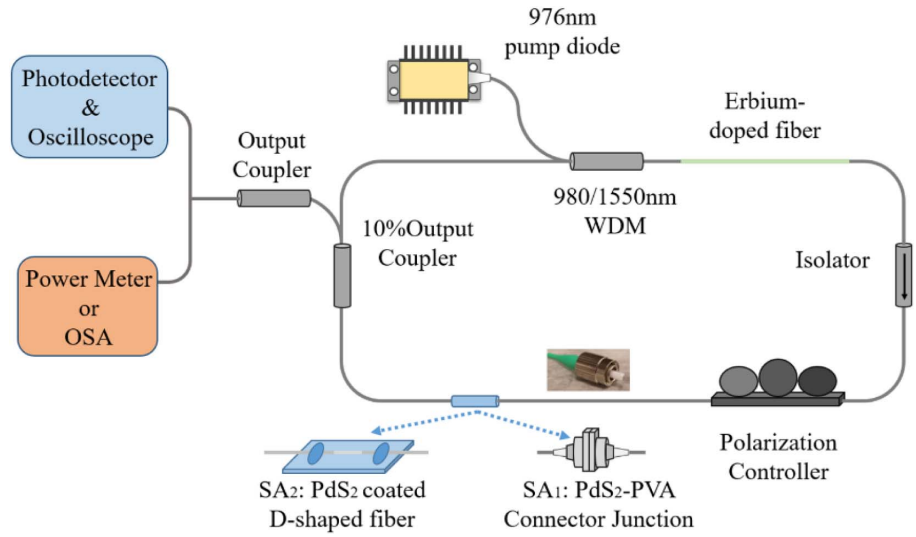

Fig. 4. Experimental setup of passively Q-switched and mode-locked EDFL cavity.

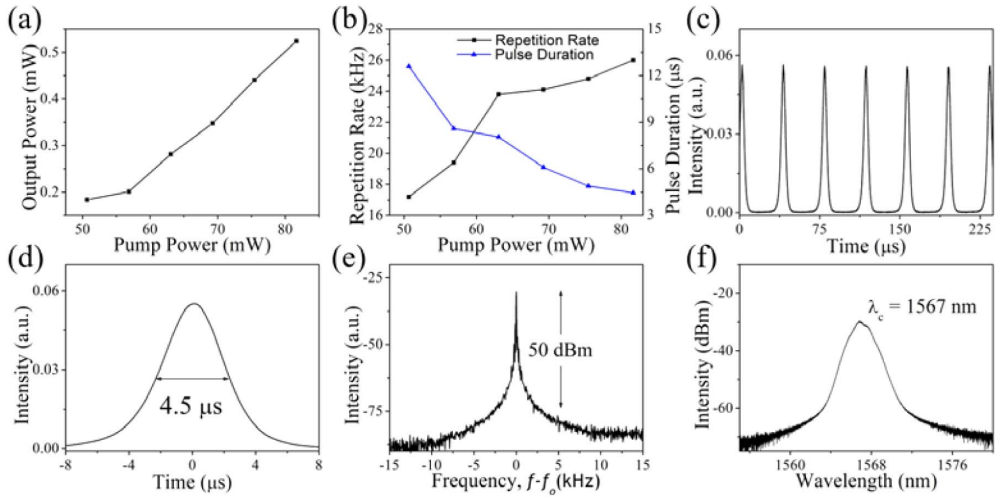

Fig. 5. Optical performance of Q-switched operation. (a) Average output power; (b) repetition rate and pulse duration regarding various optical pump powers; (c) pulse train; (d) single-pulse profile; (e) RF spectrum; and (f) wavelength spectrum at the maximum average output power.

method was also conducted in the experiment, in which the exfoliated PdS_2 samples were directly deposited onto the surface of a side-polished fiber (SPF) to form an SPF-based PdS_2-SA. The polarization-dependent loss (PDL) and the insertion loss of the SPF-based PdS_2-SA are about 2.9 and 10.1 dB, respectively. The PDL of the SPF-based PdS_2-SA is comparable to results in the previous literature, which utilized SPF and other low-dimensional materials to synthesize practical mode lockers, for instance, WS_2, 2.2 dB [47]/3 dB [48], and single-wall carbon nanotubes (SWCNTs), 5.56 dB [49]. According to the work of Zapata *et al.* [50], the PDL of SPF-based SA is affected by several parameters, including the polishing depth of SPF, the interaction length between the evanescent field and the SA materials, crystallinity or defect of the deposited SA materials, and especially the alignment direction of the 1D (SWCNTs) or 2D (TMDs) SA material [51]. To reduce the PDL, it can reduce the polishing depth of SPF or the material interaction length, and vice versa. Meanwhile, by using a balanced twin-detector system with a mode-locked laser source of 2.09 ps pulse duration and 1560 nm center wavelength, the saturable absorption characteristics of the SPF-based PdS_2-SA were quantified; they are shown in Fig. 6. The nonlinear transmission response of the PdS_2 SA was measured according to the different polarization conditions within the SPF, where the maximum and minimum recorded values of the PdS_2-SA modulation depth are shown in Figs. 6(a) and 6(b), respectively. The experimental data were fitted by using Eq. (1), where $T(I)$ is the transmittance, I_{sat} is the saturable intensity, ΔT is the modulation depth, and T_{ns} is the nonsaturation loss [37]. The saturable intensity

Table 1. Comparison of Mode-Locked and *Q*-Switched Lasers Based on Group 10 TMD SAs

	Materials	Gain Media	Wavelength	Pulse Duration	Modulation Depth	References
Mode locking						
	PtS_2	EDF	1572 nm	2.06 ps	7%	[37]
	$PtSe_2$	EDF	1560 nm	1.02 ps	4.9%	[39]
	$PtSe_2$	EDF	1567 nm	861 fs	6.96%	[40]
	$PtSe_2$	Nd:$LuVO_4$	1067 nm	15.8 ps	12.6%	[13]
	$PtSe_2$	Nd:YAG	1064 nm	27 ps	1.9%	[34]
	PdS_2	EDF	1565.8 nm	803 fs	1.7%	This work
Q switching						
	PtS_2	EDF	1569 nm	4.2 μs	/	[38]
	$PtSe_2$	EDF	1560 nm	0.9 μs	4.9%	[39]
	$PtTe_2$	YDF	1066 nm	5.2 μs	/	[41]
	PdS_2	EDF	1567 nm	4.5 μs	/	This work

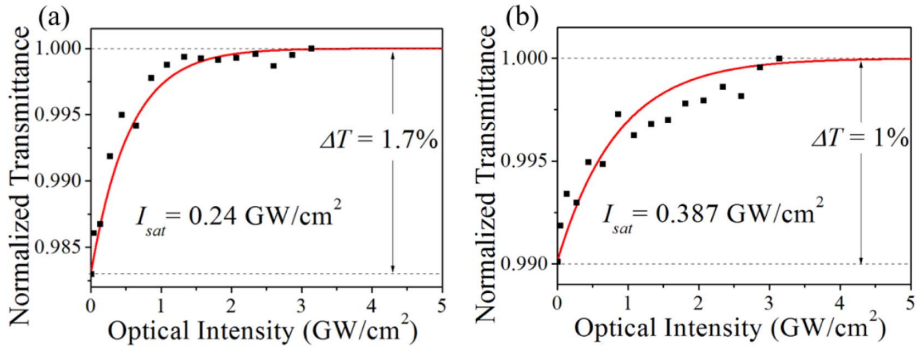

Fig. 6. Nonlinear input intensity-dependent normalized transmittance curve of PdS_2-SA at 1564 nm, the recorded (a) maximum and (b) minimum modulation depth condition according to the variation of the polarization state of input light.

and modulation depth of the SPF based PdS_2-SA are around 0.24 GW/cm^2 and 1.7%, respectively, measured in TE mode,

$$T(I) = 1 - \Delta T \cdot \exp(-I/I_{\text{sat}}) - T_{\text{ns}}. \quad \textbf{(1)}$$

By modifying the intracavity polarization state with the PC, stable CW mode-locked operation was observed as the pump power scaled beyond 106.4 mW. As shown in Fig. 7(a), the highest achieved average output power is about 0.55 mW, corresponding to the pump power of 246 mW. The average output power can be further scaled up by modifying the length of the doped fiber or utilizing the postamplification system to amplify the output signal. The measured repetition rate of the

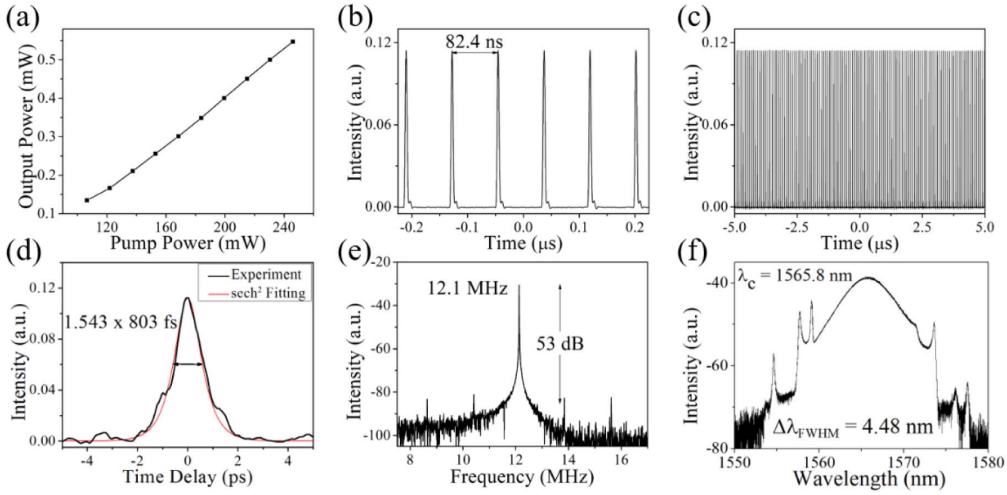

Fig. 7. Optical performance of mode-locked operation. (a) Average output power regarding various optical pump powers; (b) and (c) are pulse trains with different time scales; (d) autocorrelation trace of mode-locked pulse; (e) RF spectrum; and (f) wavelength spectrum at 0.55 mW output power.

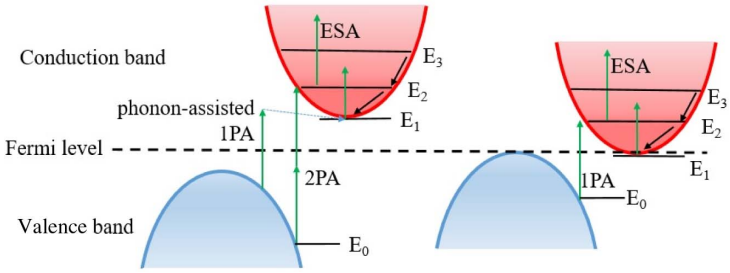

Fig. 8. Schematic diagram illustrating the photon absorption process within a four-energy level model, where the E_0, E_1, E_2, and E_3 are the ground state, first, second, and third excited state, respectively. 1PA and 2PA represent the single-photon absorption and two-photon absorption, respectively. ESA stands for the excited-state absorption.

output pulses [Fig. 7(b)] is well matched with the round-trip time and total cavity length, which proved the successful mode-locked operation. Meanwhile, from Fig. 7(c), the regular CW envelope of the output pulse train also suggested stable CW mode locking. The pulse duration was measured by using an autocorrelator (FR-103XL, Femtochrome Research, Inc.), and the result was fitted by using the squared hyperbolic secant function. As shown in Fig. 7(d), the FWHM is about 1.24 ps, which indicated that the real pulse duration is about 803 fs.

In Fig. 7(e), the fundamental repetition rate of the RF spectrum is given as about 12.1 MHz. The SNR is up to 53 dB, which also indicated that the system consists high operation stability. The wavelength spectrum illustrated the central wavelength and 3 dB bandwidth of 1565.8 and 4.48 nm, respectively, as shown in Fig. 7(f). Meanwhile, the time bandwidth product was estimated as 0.44, indicating that the pulse duration can be further improved. The output stability of the SPF-PdS_2 SA-based mode-locked laser was also studied, where the fluctuation of the average output power was less than 5% within the 30–45 min measuring period. To the best of our knowledge, this is the first demonstration of mode-locked EDFL based on palladium-TMD SAs. As shown in Table 1, the achieved pulse duration in this work is the narrowest among all other group 10 TMD SA-based results, indicating that the PdS_2-SA fabricated in this work is an advanced and promising NLO device. Wang *et al.* [52] demonstrated that the nonlinear optical absorption (NOA) response of $PtSe_2$, which has a tunable energy bandgap from 1.2 eV (indirect) of the monolayer to 0 eV of around 55 layers, is attributed to both single-photon absorption (1PA), two-photon absorption (2PA), and excited-state absorption (ESA) effects, as shown in Fig. 8. For the $PtSe_2$ in a few-layer condition (4–7 layers, 0.87 to 0.59 eV), saturable absorption is recorded as the sample interacting with a 515 nm excitation light (340 fs) in the Z-scan measurement. Nevertheless, under the excitation with a 1030 nm light, the few-layered $PtSe_2$ had demonstrated reverse saturable absorption (RSA) instead. Under the optical excitation with low photon energy, 2PA and the induced ESA will be dominant in the overall NOA effect and thus demonstrate the RSA response eventually. However, as the layer thickness increased to around 55 layers, where the $PtSe_2$ transits into semimetal behavior due to the suppression of 2PA and the domination of the 1PA effect, the NOA response of the $PtSe_2$ sample switched to saturable absorption as the incident fluence reached saturation intensity. This NOA mechanism can also be applied to the case of the semimetallic PdS_2 in this work, where the multilayered PdS_2-based SA is expected to have extensive saturable absorption response within the infrared region. In fact, we obtained a preliminary result of applying the multilayered PdS_2-based SA in a 1 μm ytterbium-doped fiber laser system recently. And it is worth further exploring the applicability of the PdS_2-SA in different laser systems, as well as deeper study of the excited carrier dynamics of this novel material in future work.

5. CONCLUSION

Passively *Q*-switched and mode-locked EDFLs were first demonstrated by using PdS_2-SAs. Self-starting *Q*-switching operation at 1567 nm was achieved with a threshold pump power of 50.6 mW. The modulation ranges of pulse duration and repetition rate were 12.6 to 4.5 μs and 17.2 to 26.0 kHz, respectively. The achieved highest average output power was 0.393 mW, corresponding to 15.1 nJ maximum single-pulse energy. Meanwhile, a mode-locked EDFL was also obtained with a pump power threshold of 106.4 mW. The achieved pulse duration of the mode-locked EDFL in this work was 803 fs, which is the narrowest result among all other group 10 TMD-SA-based lasers. This suggests the PdS_2-SA is a promising 2D materials candidate for use in NLO applications.

Funding. Research Grants Council, University Grants Committee of Hong Kong, China (GRF 152109/16E PolyU B-Q52T).

Disclosures. The authors declare no conflicts of interest.

†These authors contributed equally to this work.

REFERENCES

1. C. Leone, V. Lopresto, and I. D. Iorio, "Wood engraving by *Q*-switched diode-pumped frequency-doubled Nd:YAG green laser," Opt. Laser Eng. **47**, 161–168 (2009).
2. C. Leone, S. Genna, G. Caprino, and I. D. Iorio, "AISI 304 stainless steel marking by a *Q*-switched diode pumped Nd:YAG laser," J. Mater. Process. Technol. **210**, 1297–1303 (2010).
3. M. Skorczakowski, J. Swiderski, W. Pichola, P. Nyga, A. Zajac, M. Maciejewska, L. Galecki, J. Kasprzak, S. Gross, A. Heinrich, and T. Bragagna, "Mid-infrared *Q*-switched Er:YAG laser for medical applications," Laser Phys. Lett. **7**, 498–504 (2010).

4. A. Zajac, M. Skorczakowski, J. Swiderski, and P. Nyga, "Electrooptically *Q*-switched mid-infrared Er:YAG laser for medical application," Opt. Express **12**, 5125–5130 (2004).
5. F. Dausinger, H. Lubatschowski, and F. Lichtner, *Femtosecond Technology for Technical and Medical Applications* (Springer, 2004).
6. P. P. Pronko, P. A. VanRompay, C. Horvath, F. Loesel, T. Juhasz, X. Liu, and G. Mourou, "Avalanche ionization and dielectric breakdown in silicon with ultrafast laser pulses," Phys. Rev. B **58**, 2387–2390 (1998).
7. H. Zhang, S. Virally, Q. Bao, L. K. Ping, S. Massar, N. Godbout, and P. Kockaert, "Z-scan measurement of the nonlinear refractive index of graphene," Opt. Lett. **37**, 1856–1858 (2012).
8. H. Long, L. Tao, C. P. Chiu, C. Y. Tang, K. H. Fung, Y. Chai, and Y. H. Tsang, "The WS_2 quantum dot: preparation, characterization and its optical limiting effect in polymethylmethacrylate," Nanotechnology **27**, 414005 (2016).
9. J. K. Jabczynski, W. Zendzian, and J. Kwiatkowski, "*Q*-switched mode-locking with acousto-optic modulator in a diode pumped Nd:YVO_4 laser," Opt. Express **14**, 2184–2190 (2006).
10. D. D. Hudson, K. W. Holman, R. J. Jones, S. T. Cundiff, J. Ye, and D. J. Jones, "Mode-locked fiber laser frequency-controlled with an intracavity electro-optic modulator," Opt. Lett. **30**, 2948–2950 (2005).
11. D. H. Sutter, G. Steinmeyer, L. Gallmann, N. Matuschek, F. Morier-Genoud, U. Keller, V. Scheuer, G. Angelow, and T. Tschudi, "Semiconductor saturable-absorber mirror-assisted Kerr-lens mode-locked Ti:sapphire laser producing pulses in the two-cycle regime," Opt. Lett. **24**, 631–633 (1999).
12. J. Dong, P. Deng, Y. Liu, Y. Zhang, J. W. Chen, and X. Xie, "Passively *Q*-switched Yb:YAG laser with Cr^{4+}:YAG as the saturable absorber," Appl. Opt. **40**, 4303–4307 (2001).
13. L. Tao, X. Huang, J. He, Y. Lou, L. Zeng, Y. Li, H. Long, J. Li, L. Zhang, and Y. H. Tsang, "Vertically standing $PtSe_2$ film: a saturable absorber for a passively mode-locked Nd:$LuVO_4$ laser," Photon. Res. **6**, 750–755 (2018).
14. Z. Sun, T. Hasan, F. Torrisi, D. Popa, G. Privitera, F. Wang, F. Bonaccorso, D. M. Basko, and A. C. Ferrari, "Graphene mode-locked ultrafast laser," ACS Nano **4**, 803–810 (2010).
15. J. Wang, Z. Luo, M. Zhou, C. Ye, H. Fu, Z. Cai, H. Cheng, H. Xu, and W. Qi, "Evanescent-light deposition of graphene onto tapered fibers for passive *Q*-switch and mode-locker," IEEE Photon. J. **4**, 1295–1305 (2012).
16. Y. G. Wang, H. R. Chen, X. M. Wen, W. F. Hsieh, and J. Tang, "A highly efficient graphene oxide absorber for *Q*-switched Nd:$GdVO_4$ lasers," Nanotechnology **22**, 455203 (2011).
17. J. Xu, J. Liu, S. Wu, Q. H. Yang, and P. Wang, "Graphene oxide mode-locked femtosecond erbium-doped fiber lasers," Opt. Express **20**, 15474–15480 (2012).
18. Y. Chen, G. Jiang, S. Chen, Z. Guo, X. Yu, C. Zhao, H. Zhang, Q. Bao, S. Wen, D. Tang, and D. Fan, "Mechanically exfoliated black phosphorus as a new saturable absorber for both *Q*-switching and mode-locking laser operation," Opt. Express **23**, 12823–12833 (2015).
19. J. Sotor, G. Sobon, M. Kowalczyk, W. Macherzynski, P. Paletko, and K. M. Abramski, "Ultrafast thulium-doped fiber laser modelocked with black phosphorus," Opt. Lett. **40**, 3885–3888 (2015).
20. K. Wu, B. Chen, X. Zhang, S. Zhang, C. Guo, C. Li, P. Xiao, J. Wang, L. Zhou, W. Zou, and J. Chen, "High-performance mode-locked and *Q*-switched fiber lasers based on novel 2D materials of topological insulators, transition metal dichalcogenides and black phosphorus: review and perspective," Opt. Commun. **406**, 214–229 (2018).
21. J. Li, N. V. Medhekar, and V. B. Shenoy, "Bonding charge density and ultimate strength of monolayer transition metal dichalcogenides," J. Phys. Chem. C **117**, 15842–15848 (2013).
22. W. Zhao, Z. Ghorannevis, L. Chu, M. Toh, C. Kloc, P. H. Tan, and G. Eda, "Evolution of electronic structure in atomically thin sheets of WS_2 and WSe_2," ACS Nano **7**, 791–797 (2012).
23. H. Long, L. Tao, C. Y. Tang, B. Zhou, Y. Zhao, L. Zeng, S. F. Yu, S. P. Lau, Y. Chai, and Y. H. Tsang, "Tuning nonlinear optical absorption properties of WS_2 nanosheets," Nanoscale **7**, 17771–17777 (2015).
24. G. Liang, L. Zeng, Y. H. Tsang, L. Tao, C. Y. Tang, P. K. Cheng, H. Long, X. Liu, J. Li, J. Qu, and Q. Wen, "Technique and model for modifying the saturable absorption (SA) properties of 2D nanofilms by considering interband exciton recombination," J. Mater. Chem. C **6**, 7501–7511 (2018).
25. H. L. Zhuang and R. G. Hennig, "Computational search for single-layer transition-metal dichalcogenide photocatalysts," J. Phys. Chem. C. **117**, 20440–20445 (2013).
26. Y. Zhao, J. Qiao, Z. Yu, P. Yu, K. Xu, S. P. Lau, W. Zhou, Z. Liu, X. Wang, W. Ji, and Y. Chai, "High-electron-mobility and air-stable 2D layered $PtSe_2$ FETs," Adv. Mater. **29**, 1604230 (2017).
27. L. H. Zeng, S. H. Lin, Z. J. Li, Z. X. Zhang, T. F. Zhang, C. Xie, C. H. Mak, Y. Chai, S. P. Lau, L. B. Luo, and Y. H. Tsang, "Fast, self-driven, air-stable, and broadband photodetector based on vertically aligned $PtSe_2$/GaAs heterojunction," Adv. Funct. Mater. **28**, 1705970 (2018).
28. L. H. Zeng, S. H. Lin, Z. H. Lou, H. Y. Yuan, H. Long, Y. Y. Li, W. Lu, S. P. Lau, D. Wu, and Y. H. Tsang, "Ultrafast and sensitive photodetector based on a $PtSe_2$/silicon nanowire array heterojunction with a multiband spectral response from 200 to 1550 nm," NPG Asia Mater. **10**, 352–362 (2018).
29. D. Wu, Y. Wang, L. H. Zeng, C. Jia, E. Wu, T. Xu, Z. Shi, Y. Tian, X. Li, and Y. H. Tsang, "Design of 2D layered $PtSe_2$ heterojunction for the high-performance room-temperature broadband infrared photodetector," ACS Photon. **5**, 3820–3827 (2018).
30. L. H. Zeng, D. Wu, S. H. Lin, C. Xie, H. Y. Yuan, W. Lu, S. P. Lau, Y. Chai, L. B. Luo, Z. J. Li, and Y. H. Tsang, "Controlled synthesis of two-dimensional palladium diselenide for sensitive photodetectors application," Adv. Funct. Mater. **29**, 1806878 (2018).
31. K. Wu, X. Zhang, J. Wang, X. Li, and J. Chen, "WS_2 as a saturable absorber for ultrafast photonic applications of mode-locked and *Q*-switched lasers," Opt. Express **23**, 11453–11461 (2015).
32. C. Y. Tang, P. K. Cheng, L. I. Tao, H. Long, L. H. Zeng, Q. Wen, and Y. H. Tsang, "Passively *Q*-switched Nd:YVO_4 laser using WS_2 saturable absorber fabricated by radio frequency magnetron sputtering deposition," J. Light. Technol. **35**, 4120–4124 (2017).
33. L. C. Kong, G. Q. Xie, P. Yuan, L. J. Qian, S. X. Wang, H. H. Yu, and H. J. Zhang, "Passive *Q*-switching and *Q*-switched mode-locking operations of 2 μm Tm:CLNGG laser with MoS_2 saturable absorber mirror," Photon. Res. **3**, A47–A50 (2015).
34. Z. Li, R. Li, C. Pang, N. Dong, J. Wang, H. Yu, and F. Chen, "8.8 GHz *Q*-switched mode-locked waveguide lasers modulated by $PtSe_2$ saturable absorber," Opt. Express **27**, 8727–8737 (2019).
35. M. Long, Y. Wang, P. Wang, X. Zhou, H. Xia, C. Luo, S. Huang, G. Zhang, H. Yan, Z. Fan, X. Wu, X. Chen, W. Lu, and W. Hu, "Palladium diselenide long-wavelength infrared photodetector with high sensitivity and stability," ACS Nano **13**, 2511–2519 (2019).
36. L. H. Zeng, Q. M. Chen, Z. X. Zhang, D. Wu, H. Yuan, Y. Y. Li, Q. Qarony, S. P. Lau, L. B. Luo, and Y. H. Tsang, "Multilayerd $PdSe_2$/perovskite Schottky junction for fast, self-powered, polarization-sensitive, broadband photodetectors, and image sensor application," Adv. Sci. **6**, 1901134 (2019).
37. H. Long, C. Y. Tang, P. K. Cheng, X. Y. Wang, W. Qarony, and Y. H. Tsang, "Ultrafast laser pulses generation by using 2D layered PtS_2 as a saturable absorber," J. Light. Technol. **37**, 1174–1179 (2018).
38. X. Wang, P. K. Cheng, C. Y. Tang, H. Long, H. Yuan, L. Zeng, S. Ma, W. Qarony, and Y. H. Tsang, "Laser *Q*-switching with PtS_2 microflakes saturable absorber," Opt. Express **26**, 13055–13060 (2018).
39. K. Zhang, M. Feng, Y. Ren, F. Liu, X. Chen, J. Yang, X. Q. Yan, F. Song, and J. Tian, "*Q*-switched and mode-locked Er-doped fiber laser using $PtSe_2$ as a saturable absorber," Photon. Res. **6**, 893–899 (2018).
40. B. Huang, L. Du, Q. Yi, L. Yang, J. Li, L. Miao, C. Zhao, and S. Wen, "Bulk-structured $PtSe_2$ for femtosecond fiber laser mode-locking," Opt. Express **27**, 2604–2611 (2019).
41. P. K. Cheng, C. Y. Tang, X. Y. Wang, S. Ma, H. Long, and Y. H. Tsang, "Passively *Q*-switched ytterbium-doped fiber laser based on broadband multilayer platinum ditelluride ($PtTe_2$) saturable absorber," Sci. Rep. **9**, 10106 (2019).
42. Y. Wang, Y. Li, and Z. Chen, "Not your familiar two dimensional transition metal disulfide: structural and electronic properties of the PdS_2 monolayer," J. Mater. Chem. C **3**, 9603–9608 (2015).
43. M. G. Asl, A. Kuc, P. Miro, and T. Heine, "A single-material logical junction based on 2D crystal PdS_2," Adv. Mater. **28**, 853–856 (2016).

44. D. Saraf, S. Chakraborty, A. Kshirsagar, and R. Ahuja, "In pursuit of bifunctional catalytic activity in PdS_2 pseudo-monolayer through reaction coordinate mapping," Nano Energy **49**, 283–289 (2018).
45. P. Kristin, *Materials Data on PdS_2 (SG:61) by Materials Project* (2014).
46. P. P. Kiran, D. R. Reddy, B. G. Maiya, A. K. Dharmadhikari, G. R. Kumar, and D. N. Rao, "Nonlinear absorption properties of axial-bonding type tin(IV) tetratolyporphyrin based hybrid porphyrin arrays," Opt. Commun. **252**, 150–161 (2005).
47. M. Jung, J. Lee, J. Park, J. Koo, Y. M. Jhon, and J. H. Lee, "Mode-locked, 1.94-μm, all-fiberized laser using WS_2-based evanescent field interaction," Opt. Express **23**, 19996–20006 (2015).
48. J. Lee, J. Park, J. Koo, Y. M. Jhon, and J. H. Lee, "Harmonically mode-locked femtosecond fiber laser using non-uniform, WS_2-particle deposited side-polished fiber," J. Opt. **18**, 035502 (2016).
49. H. Jeong, S. Y. Choi, F. Rotermund, Y. H. Cha, D. Y. Jeong, and D. I. Yeom, "All-fiber mode-locked laser oscillator with pulse energy of 34 nJ using a single-walled carbon nanotube saturable absorber," Opt. Express **22**, 22667–22672 (2014).
50. J. D. Zapata, D. Steinberg, L. A. Saito, R. E. P. De Oliveira, A. M. Cárdenas, and E. T. De Souza, "Efficient graphene saturable absorbers on D-shaped optical fiber for ultrashort pulse generation," Sci. Rep. **6**, 20644 (2016).
51. Y. W. Song, S. Yamashita, E. Einarsson, and S. Maruyama, "All-fiber pulsed lasers passively mode locked by transferable vertically aligned carbon nanotube film," Opt. Lett. **32**, 1399–1401 (2007).
52. L. Wang, S. Zhang, N. McEvoy, Y. Y. Sun, J. Huang, Y. Xie, and L. Zhang, "Nonlinear optical signatures of the transition from semiconductor to semimetal in $PtSe_2$," Laser Photon. Rev. **13**, 1900052 (2019).